ACS APPLIED MATERIALS & INTERFACES

Research Article

www.acsami.org

Measurement of Small Molecular Dopant F4TCNQ and $C_{60}F_{36}$ Diffusion in Organic Bilayer Architectures

Jun Li,[†] Chris W. Rochester,[†] Ian E. Jacobs,[†] Stephan Friedrich,[‡] Pieter Stroeve,[†] Moritz Riede,[§] and Adam J. Moulé*,[†]

[†]Department of Chemical Engineering and Materials Science, University of California, Davis, California 95616, United States

[‡]Lawrence Livermore National Laboratory, Livermore, California 94550, United States

[§]Department of Physics, Oxford University, Oxford OX1 3PU, United Kingdom

Supporting Information

ABSTRACT: The diffusion of molecules through and between organic layers is a serious stability concern in organic electronic devices. In this work, the temperature-dependent diffusion of molecular dopants through small molecule hole transport layers is observed. Specifically we investigate bilayer stacks of small molecules used for hole transport (MeO-TPD) and p-type dopants (F4TCNQ and $C_{60}F_{36}$) used in hole injection layers for organic light emitting diodes and hole collection electrodes for organic photovoltaics. With the use of absorbance spectroscopy, photoluminescence spectroscopy, neutron reflectometry, and near-edge X-ray absorption fine structure spectroscopy, we are able to obtain a comprehensive picture of the diffusion of fluorinated small molecules through MeO-TPD layers. F4TCNQ spontaneously diffuses into the MeO-TPD material even at room temperature, while $C_{60}F_{36}$, a much bulkier molecule, is shown to have a substantially higher morphological stability. This study highlights that the differences in size/geometry and thermal properties of small molecular dopants can have a significant impact on their diffusion in organic device architectures.

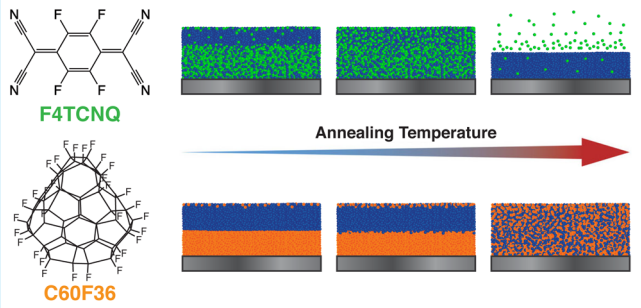

KEYWORDS: *organic light emitting diodes, organic photovoltaics, dopant, diffusion, device stability*

INTRODUCTION

A variety of organic electronic materials have been developed and successfully incorporated into electronic and optoelectronic devices for different applications.[1,2] As organic electronic devices continue to improve, more attention has to be placed on studying and improving the stability and lifetimes of these devices if they are to be commercially competitive with their inorganic counterparts.[3−7] Organic electronic devices consist of conjugated small molecule or polymer materials that are deposited to form multilayered structures. Ideally, each layer would perform a particular function (since no one material has all desired properties) without interference from neighboring layers, but usually layers have several functions. The featured doped layers in this work are typically between and in direct contact with other layers including intrinsic organic semiconductors, highly doped organic semiconductors, and/or inorganic insulating or metal layers. In order to monitor the transport of molecules between these layers and interfaces, it is important to use characterization methods that allow for the detection of low density species that may contribute to device instability.[4,6,7]

Most organic light emitting diodes (OLEDs) and organic photovoltaic devices (OPVs) incorporate dedicated charge transport layers to facilitate charge carrier injection or extraction.[8−10] Molecular doping of these layers has been one of the key enabling technologies for making OLEDs commercial, and an increasing number of OPVs are using doped transport layers as well. Doping of organic semiconductors has benefits similar to the doping of inorganic semiconductors: it allows control of the Fermi level leading, e.g., to quasi-ohmic interfaces to metals.[11−16] The doping mechanism occurs by an electron transfer process between the dopant molecule and the host material.[11,17] For p-type doping, the electron is transferred from the host material to the dopant, and for n-type doping the electron transfers from the dopant molecule to the host material. An important difference between doping inorganic semiconductors and doping organic electronic materials is that, for organic doping, the dopant molecules are not bound to their host material by strong covalent bonds. Organic molecules are held in place by weak van der Waals interactions and Coulombic attractions between charged species. Because of these weaker interactions in organic materials, the molecules themselves have higher mobilities within the host material, and therefore have a higher tendency

Received: September 30, 2015
Accepted: December 2, 2015
Published: December 3, 2015

 © 2015 American Chemical Society

DOI: 10.1021/acsami.5b09216
ACS Appl. Mater. Interfaces 2015, 7, 28420−28428

to diffuse than in inorganic semiconductors. The diffusion of dopant molecules within and between layers of a device can greatly hinder the performance by causing unwanted interactions with other materials, but there have been very few studies directly investigating this process.[11,18,19]

The first doping experiments were performed using atomic dopants such as iodine and bromine[20,21] and later using atoms such as lithium, cesium, and strontium.[22,23] However, those dopants are all too small. Larger molecular dopants were introduced to reduce diffusivity. A very common p-type dopant used in many organic electronic studies is 2,3,5,6-tetrafluoro-7,7,8,8-tetracyanoquinodimethane (F4TCNQ).[13,24−26] F4TCNQ is a fluorinated small molecule with a sufficiently high electron affinity of 5.24 eV.[24] Due to its high electron affinity, F4TCNQ is capable of oxidizing a large variety of conjugated organic materials. In OPVs and OLEDs, F4TCNQ is often used to dope hole transport layer (HTL) materials, such as *N*,*N*,*N*′,*N*′-tetrakis(4-methoxyphenyl)benzidine (MeO-TPD), shown in Figure 1. It has been demonstrated that devices that use F4TCNQ as a dopant frequently fail when the device is exposed to elevated temperatures.[18,27] These failures have been attributed to the increased diffusion rate of F4TCNQ at higher temperatures, causing the dopant molecules to diffuse into the adjacent active layer. This unwanted diffusion has led to the search for less mobile p-dopants to improve the stability of the HTLs. One of these more stable dopants is $C_{60}F_{36}$ (M_w = 1404.6 g/mol) shown in Figure 1, which is a fluorinated fullerene with an electron affinity of 5.38 eV.[28,29] The improved stability of this molecule is attributed to its larger size, making it less mobile than the much smaller F4TCNQ (M_w = 276.2 g/mol).

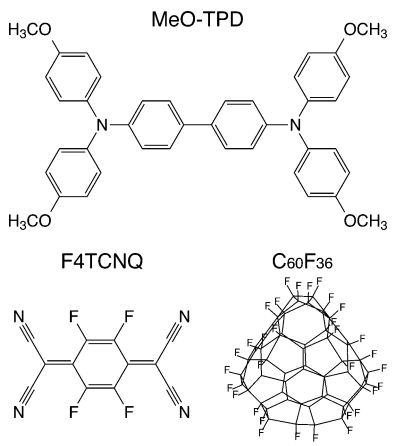

Figure 1. Molecular structures of hole transport molecule MeO-TPD and p-type molecular dopants F4TCNQ and $C_{60}F_{36}$.

In this work, we investigate the optical consequences of dopant diffusion using UV−vis−near-IR and photoluminescence spectroscopies. A comprehensive comparison between the diffusion of F4TCNQ and $C_{60}F_{36}$ through MeO-TPD is also performed using neutron reflectometry (NR) and near-edge X-ray absorption fine structure (NEXAFS) spectroscopy. This study highlights that the differences in size and geometry of small molecule dopants can have a significant impact on the diffusion in the device structures.

EXPERIMENTAL SECTION

Materials. MeO-TPD and F4TCNQ were purchased from Sigma-Aldrich. $C_{60}F_{36}$ was purchased from MTR Ltd. (Cleveland, OH, USA). All chemicals were used as-received unless otherwise indicated.

Measurements. *UV−Vis−Near-IR and Photoluminescence Spectroscopies.* Ultraviolet−visible−near-infrared (UV−vis−near-IR) absorbance spectra and photoluminescence (PL) spectra were recorded using a PerkinElmer Lambda 750 spectrophotometer and a Varian Eclipse photoluminescence spectrophotometer, respectively. Quartz substrates (1 in. × 1 in.) were cleaned in ultrasonic baths of acetone, Mucasol detergent (5%), and deionized water, followed by drying with nitrogen. The substrates were then exposed to UV/ozone for 30 min before use. MeO-TPD, F4TCNQ, and $C_{60}F_{36}$ were deposited using a MBraun thermal evaporator at a deposition rate ∼ 0.2 Å/s at ∼160, ∼80, and ∼180 °C, respectively. Prior to deposition, the evaporation chamber was pumped down to a pressure of 5×10^{-6} mbar. The two bilayer samples were made, one with a 30 nm MeO-TPD layer on top of 30 nm of F4TCNQ and the other with a 30 nm MeO-TPD layer on top of 30 nm of $C_{60}F_{36}$. In order to eliminate cross-contamination, only one material was deposited at a time and the evaporation chamber was pressurized and opened in order to switch evaporation crucibles between each evaporation. Spectra on single layers of each of the neat materials (MeO-TPD, F4TCNQ, and $C_{60}F_{36}$) were also obtained for reference. Film thicknesses were measured using a Veeco Dektak 150 surface profilometer. The samples were annealed at elevated temperatures for 5 min on a digital hot plate inside a nitrogen glovebox. All UV−vis−near-IR and PL spectra were measured under ambient conditions in air.

Neutron Reflectometry. Neutron reflectometry measurements were performed on the surface profile analysis reflectometer (SPEAR) flight path at the Manuel Lujan, Jr. Neutron Scattering Center at Los Alamos National Laboratory.[30] Silicon wafers (3 in. diameter) were used as substrates. The same procedure was used for substrate cleaning and thermal evaporation as described previously. All of the reflectometry measurements were performed in air. The bilayer samples were measured before and after heating at 110 °C for 5 min.

For the neutron reflectometry measurements, the reflected beam intensity was measured as a function of scattering vector (q_z),

$$q_z = \frac{4\pi}{\lambda} \sin \theta_i \tag{1}$$

where λ is the wavelength of the incident beam and θ_i is the incident angle, which is defined as the angle between the beam and the surface plane of the sample. The reflectivity data were analyzed using the MOTOFIT reflectometry analysis package within the IGOR software.[31] A slab model was used to represent the samples. The fit parameters used to characterize each layer in the model include thickness, scattering length density (SLD), and interlayer roughness. SLD is defined as

$$\mathrm{SLD} = \frac{\sum_{i=1}^{N} b_i}{V_m} = \frac{\rho N_A}{M_w} \sum_{i=1}^{N} b_i \tag{2}$$

where V_m is the molecular volume, ρ is the mass density of the material, N_A is Avogadro's number, M_w is the molecular weight, and b_i is the neutron scattering length of atom i for a molecule containing N atoms. The SLDs of silicon and air were taken to be 2.07×10^{-6} Å^{-2} and 0 Å^{-2}, respectively.[32] During the fitting process, the layer parameters are systematically varied until a fit between the model reflectivity and the measured reflectivity is produced. The resultant fit produces a vertical SLD profile of the measured sample.

Near-Edge X-ray Absorption Fine Structure Spectroscopy. Near-edge X-ray absorption fine structure measurements were performed on Beamline 6.3.1 at the Advanced Light Source (ALS) at Lawrence Berkeley National Laboratory. Samples were prepared by thermal evaporation onto ITO-coated glass. In addition to the bilayer samples with MeO-TPD on top, inverse bilayer structures for both dopants were also prepared following the same procedure described earlier. The samples were then divided into nine (1/3 × 1/3 in.^{2}) subsections,

DOI: 10.1021/acsami.5b09216
ACS Appl. Mater. Interfaces 2015, 7, 28420−28428

and each piece was heated at various temperatures in a nitrogen glovebox for 5 min before the measurements. The carbon K-edge spectra were obtained by total electron yield (TEY) at X-ray incidence angle ~30° using a Galileo 4716 channeltron electron multiplier, and the TEY signal was normalized by the incident beam intensity I_0. The data were processed and analyzed using Athens software, where a linear background was subtracted, and the spectra were normalized above the edge at 310 eV. The energy was also calibrated by setting the strong resonance peak corresponding to C 1s (C═C) → $\pi^*_{C=C}$ to 285.2 eV.[33]

■ RESULTS AND DISCUSSION

Optical Consequences of Dopant Diffusion. In order to observe the diffusion of a dopant upon thermal annealing, it is necessary to (a) prepare a sample in which the initial location of the dopant is known and (b) nondestructively detect the dopant at low concentrations within the background of the host material. The former can be achieved by properly preparing samples. Since optical absorption spectroscopy (UV−vis−near-IR) is commonly used to observe charge transfer between host molecules and dopants,[25,34,35] it will allow us to qualitatively observe the dopant diffusion.

In this section, the diffusion of F4TCNQ in MeO-TPD is first investigated. In order to eliminate cross-contamination of F4TCNQ due to its high volatility, only one material was deposited at a time and the chamber was pressurized and opened for switching crucibles between each evaporation step. In addition, a control experiment was also performed (Supporting Information Figure S1). The results of no presence of F4TCNQ in MeO-TPD UV−vis−near-IR spectra and no noticeable quenching in photoluminescence spectra indicate that the F4TCNQ background doping (either from re-evaporation from the walls or sequential deposition) has negligible effect on our results. The UV−vis−near-IR absorbance spectra of a bilayer of a 30 nm MeO-TPD layer on top of 30 nm of F4TCNQ before and after annealing at various temperatures are shown in Figure 2a. The absorbance spectra of the individual layers of the two materials are also given. As can be seen, the F4TCNQ film is identified by the absorption peaks at 2.82 eV while the MeO-TPD film is identified at 3.38 and 4.0 eV, which correspond to the $\pi-\pi^*$ absorbance.[36] In the as-cast bilayer sample, the features of both materials are discernible. Upon thermal annealing, additional low energy transition peaks appear, which consist of two broad absorption peaks centered at 0.79 and 2.62 eV which we assign to the MeO-TPD polarons, along with two other peaks at 1.43 and 1.63 eV, which are characteristic of F4TCNQ anion.[37−40] The depletion of MeO-TPD and F4TCNQ is attributed to the charge transfer between these two molecules, which results in the charged species MeO-TPD$^+$ and F4TCNQ$^-$. To keep track of the charge transfer reaction which will eventually allow us to monitor the dopant diffusion in the binary system, the changes in peak intensity of neutral molecules and charged species extracted from UV−vis−near-IR spectra under elevated temperatures are shown in Figure 2b. For the initial unheated sample, the absorption peaks for F4TCNQ$^-$ (1.43 eV) and MeO-TPD$^+$ (0.79 and 2.62 eV) can still be detected, although they are very small. The presence of these charged species before heating is likely due to the doping reaction that occurs at the interface of these two layers. Upon thermal annealing to 110 °C, the absorption peaks of the neutral molecules (3.38 and 4.0 eV) decrease dramatically and the peaks for the charged molecules (0.79, 1.43, and 2.62 eV) reach their maximum, showing that there is a substantial amount of diffusion-induced

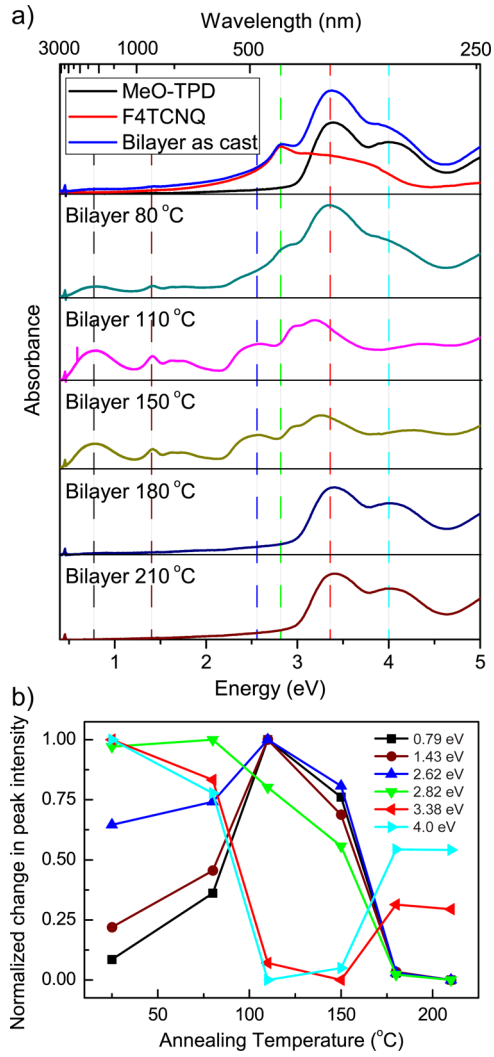

Figure 2. (a) UV−vis−near-IR spectra of MeO-TPD (black), F4TCNQ (red), and bilayers of 30 nm MeO-TPD thermally evaporated onto 30 nm of F4TCNQ. The bilayer spectra are displayed as deposited (blue) and after heating to 80 °C (cyan), 110 °C (magenta), 150 °C (dark yellow), 180 °C (navy), and 210 °C (wine). (b) Normalized changes in peak intensity of neutral molecules (2.82, 3.38, and 4.0 eV) and charged species (0.79, 1.43, and 2.62 eV) extracted from UV−vis−near-IR spectra under elevated temperatures.

doping caused by the diffusion of F4TCNQ molecules into the MeO-TPD layer, vice versa, or both. Interestingly, once the annealing temperature passes 150 °C, all of these charge transfer features disappear and the spectra seem to be almost the same as the pristine MeO-TPD film. This was expected since F4TCNQ is known as a highly volatile molecule and is very likely to evaporate at such high temperature.[28,41] This drawback had been shown to cause serious issues when using a F4TCNQ doped hole transporting layer (HTL) such as cross-contamination and thermal instability of the organic device.[27,42,43]

Figure 3a shows the absorbance spectra of a bilayer consisting of MeO-TPD evaporated on top of a layer of $C_{60}F_{36}$ before and after annealing at various temperatures, and similarly, the changes in peak intensity of neutral molecules and charged species under elevated temperatures are also presented (Figure 3b). Within the displayed measurement range, the $C_{60}F_{36}$ is almost completely transparent, so the spectrum is

DOI: 10.1021/acsami.5b09216
ACS Appl. Mater. Interfaces 2015, 7, 28420−28428

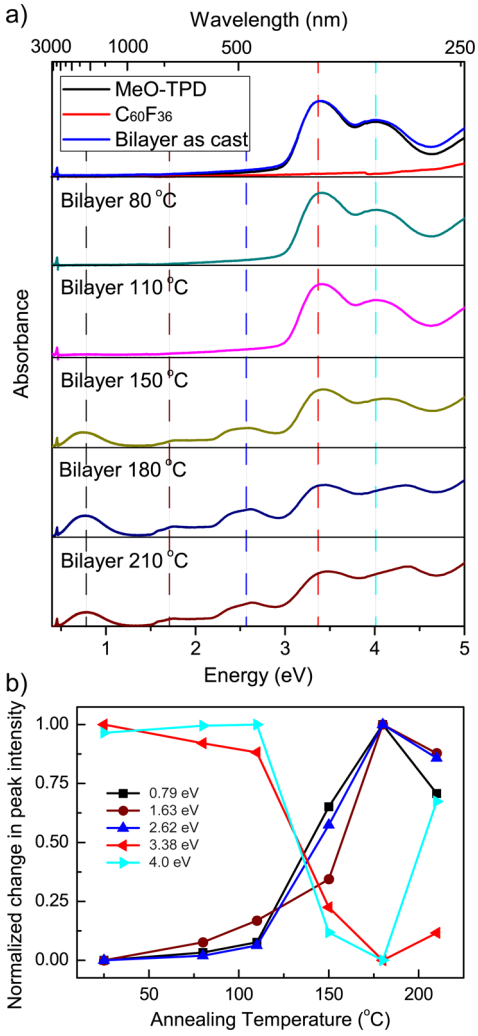

Figure 3. (a) UV−vis−near-IR spectra of MeO-TPD (black), $C_{60}F_{36}$ (red), and bilayers of 30 nm MeO-TPD thermally evaporated onto 30 nm of $C_{60}F_{36}$. The bilayer spectra are displayed as deposited (blue) and after heating to 80 °C (cyan), 110 °C (magenta), 150 °C (dark Yellow), 180 °C (navy), and 210 °C (wine). (b) Normalized changes in peak intensity of neutral molecules (3.38 and 4.0 eV) and charged species (0.79, 1.63, and 2.62 eV) extracted from UV−vis−near-IR spectra under elevated temperatures.

dominated by the MeO-TPD. The initial spectrum of the sample shows no sign of doping as there are no peaks other than the neutral MeO-TPD peaks, which implies that discrete $C_{60}F_{36}$ and MeO-TPD layers are formed. Heating the $C_{60}F_{36}$/MeO-TPD bilayer sample at 80 and 110 °C for 5 min shows no significant change, which can be seen clearly in Figure 3b. Such subtle change is probably a result of the interfacial doping effect of two materials. This lack of change in the spectrum shows that the $C_{60}F_{36}$ is much more stable with respect to diffusion than F4TCNQ. After heating the sample to 150 °C, the $C_{60}F_{36}$ becomes mobile and the two layers start mixing, which initializes the doping reaction, producing $C_{60}F_{36}^{-}$ and MeO-TPD^{+}. The difference of the new peak positions around 1.5 eV and similarity of the two broad absorption peaks at 0.79 and 2.62 eV in both systems allow us to assign these two broad low energy absorbances to MeO-TPD^{+} and the peaks in the red to the dopant anions. In addition, the neutral MeO-TPD absorptions are also depleted. Further increasing the annealing temperature eases the diffusion of dopants. Unlike F4TCNQ, $C_{60}F_{36}$ does not sublimate under thermal stress due to its low volatility and high thermal stability.[28]

Photoluminescence (PL) spectroscopy is another technique that has been extensively used to investigate the effect of doping interactions since the photoluminescence of the host material is quenched by the presence of dopants.[29,44,45] Specifically in our case, the PL quenching of MeO-TPD can result from several different mechanisms, such as positive polarons quenching the excitations in the MeO-TPD, energy transfer from the MeO-TPD to the dopants, and possibly photoinduced electron transfer processes from the MeO-TPD to the dopant. Although we do not intend to separate these mechanisms in this work, we can still apply PL technique to observe the dopant diffusion. The PL measurements were performed using 3.38 eV excitation to optically excite MeO-TPD, and the PL emission for undoped domains (2.1−3.3 eV) was observed. The normalized PL quantum efficiencies (PLQE) of two bilayer systems under elevated temperatures are shown in Figure 4. As can be seen, before annealing over

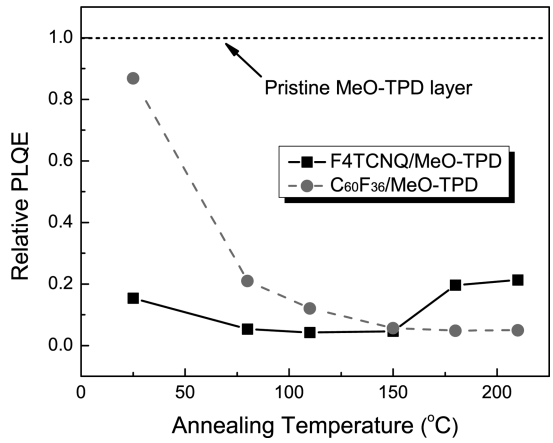

Figure 4. Relative photoluminescence quantum efficiency (PLQE) of F4TCNQ/MeO-TPD bilayer (solid line, square symbols) and $C_{60}F_{36}$/MeO-TPD bilayer (dashed line, round symbols) as a function of annealing temperature. Photoluminescence quenching is normalized by PL intensity of the pristine MeO-TPD layer.

80% PL intensity is quenched in F4TCNQ/MeO-TPD, while only partial PL quenching of ∼10% is observed in $C_{60}F_{36}$/MeO-TPD. Given the short exciton diffusion length in MeO-TPD, this result clearly shows that substantial diffusion and doping have already taken place for F4TCNQ even at room temperature. In addition, we also note that the PL quenching of F4TCNQ/MeO-TPD is much faster than that of $C_{60}F_{36}$/MeO-TPD at the same annealing conditions. Unlike F4TCNQ/MeO-TPD, where complete quenching occurs at around 80 °C, complete quenching for $C_{60}F_{36}$/MeO-TPD is observed at around 150 °C. This is consistent with UV−vis−near-IR results, where a lag in the bleaching of neutral molecules absorbances and the appearance of charged species peaks is observed in $C_{60}F_{36}$/MeO-TPD. Interestingly, the PL intensity of F4TCNQ/MeO-TPD is recovered by ∼20% once the annealing temperature passes 150 °C, which is also attributed to the high volatility of F4TCNQ molecules. The incomplete recovery of PL intensity also indicates that residual F4TCNQ still exists in the MeO-TPD in the doped form. The full temperature-dependent PL spectra of both systems can be found in the Supporting Information (Figure S2).

DOI: 10.1021/acsami.5b09216
ACS Appl. Mater. Interfaces 2015, 7, 28420−28428

Measurement of Dopant Diffusion. The preceding section has shown that UV−vis−near-IR and PL spectroscopies are straightforward techniques than can be used to observe the diffusion of a dopant upon thermal annealing. However, neither of them can provide information on either the new distribution of dopant locations or the diffusion direction. In this section, NR and NEXAFS spectroscopies will be introduced to accomplish this purpose.

Neutron Reflectometry. Neutron reflectivity measurements provide information about the vertical composition profile of the film. Both chosen dopants are fully fluorinated and have no hydrogens. Since hydrogen has a negative scattering length (−3.739 fm) for neutrons while fluorine has a positive length (5.654 fm),[32] the fluorinated dopants are able to provide a high scattering contrast to the HTL materials. The neutron reflectivity curves for a 30 nm layer of MeO-TPD deposited onto a 5 nm layer of F4TCNQ are shown in Figure 5a. An expected reflectivity produced from a two-layer reflectometry model is also given. From fit reflectivity data for a single layer of the MeO-TPD sample, the SLD of MeO-TPD was determined to be 2.05×10^{-6} Å^{-2}, which corresponds to a mass density of 1.2 g/cm^3. The SLD for F4TCNQ was calculated to be 4.88×10^{-6} Å^{-2} using a mass density value of 1.6 g/cm^3.

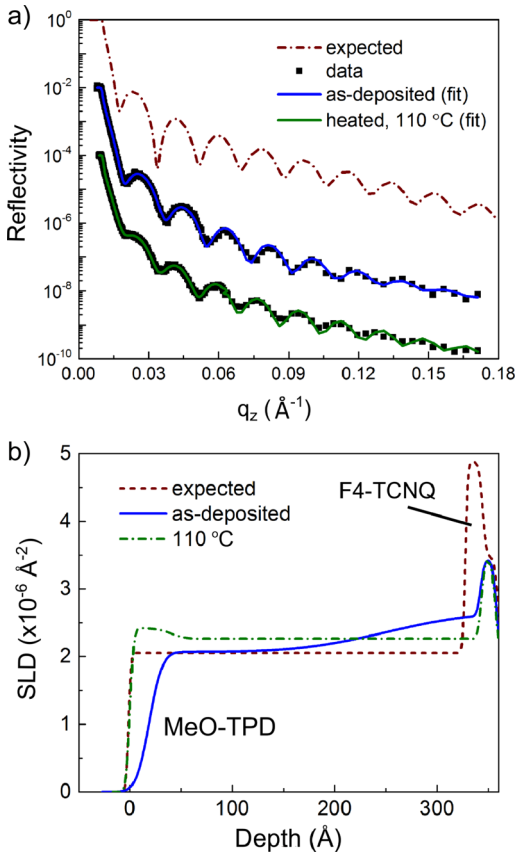

Figure 5. Neutron reflectometry data and model fits (a) and scattering length density (SLD) profiles (b) of a bilayer of MeO-TPD (30 nm) thermally evaporated onto 5 nm of F4TCNQ as deposited (blue) and after heating to 110 °C (green).

Figure 5b shows the SLD profile for the sample obtained from fitting the reflectivity data, along with the expected initial profile. The surface of the sample is shown to the left of the plot at a depth of 0 Å, and the right of the plot is the base of the sample, where the SiO_2 layer of the substrate is seen as a peak at a depth of 350 Å with an SLD value of 3.45×10^{-6} Å^{-2}. As can be seen, the SLD profile of the as-cast sample does not show two distinct layers as expected. Instead, a diffuse high SLD layer that extends into the MeO-TPD layer is formed, indicating that F4TCNQ has already diffused into the MeO-TPD layer at room temperature. Note that there is no contradiction between the spectroscopy and neutron results for unheated samples, since the spectroscopy was performed within 1 h after the sample was made, while the neutron samples were made several days before measurement and were transported by plane to Los Alamos. The F4TCNQ diffuses very slowly at room temperature, but with large accumulated results. Also shown in Figure 5b is the reflectometry result of the sample heated at 110 °C for 5 min. It is observed that, after thermal annealing, the F4TCNQ diffuses throughout the MeO-TPD layer. The high SLD surface that appears after heating the sample is a result of the F4TCNQ accumulating at the surface, which is likely due to the low surface energy of the fluorinated molecules and some thermal oxidation. The effect of increased surface SLD was also reported in earlier publications.[46,47]

The neutron reflectivity curves and the SLD profiles for a bilayer of a 30 nm layer of MeO-TPD on a 30 nm layer of $C_{60}F_{36}$ before and after annealing are shown in Figure 6. From fit reflectivity data for a single layer, the SLD of $C_{60}F_{36}$ was determined to be 4.85×10^{-6} Å^{-2}, which corresponds to a mass density of 1.9 g/cm^3. The as-deposited sample profile clearly shows that these two layers do not mix before annealing. The

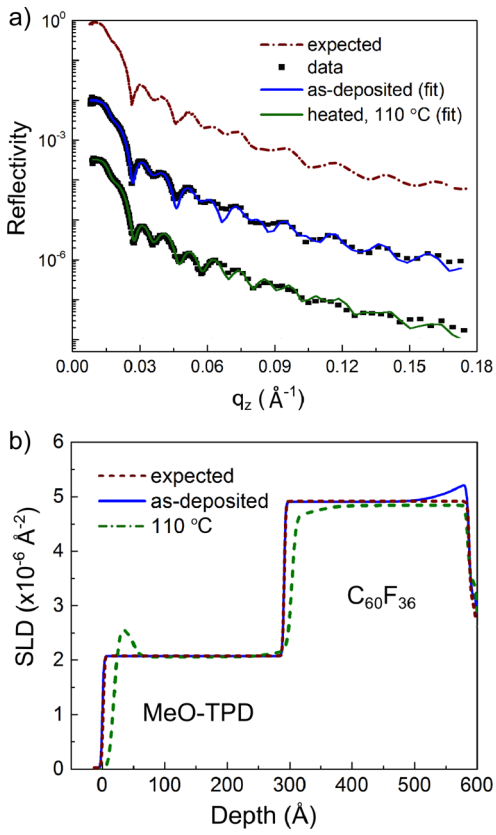

Figure 6. Neutron reflectometry data and model fits (a) and scattering length density (SLD) profiles (b) of a bilayer of MeO-TPD (30 nm) thermally evaporated onto 30 nm of $C_{60}F_{36}$ as deposited (blue) and after heating to 110 °C (green).

DOI: 10.1021/acsami.5b09216
ACS Appl. Mater. Interfaces 2015, 7, 28420−28428

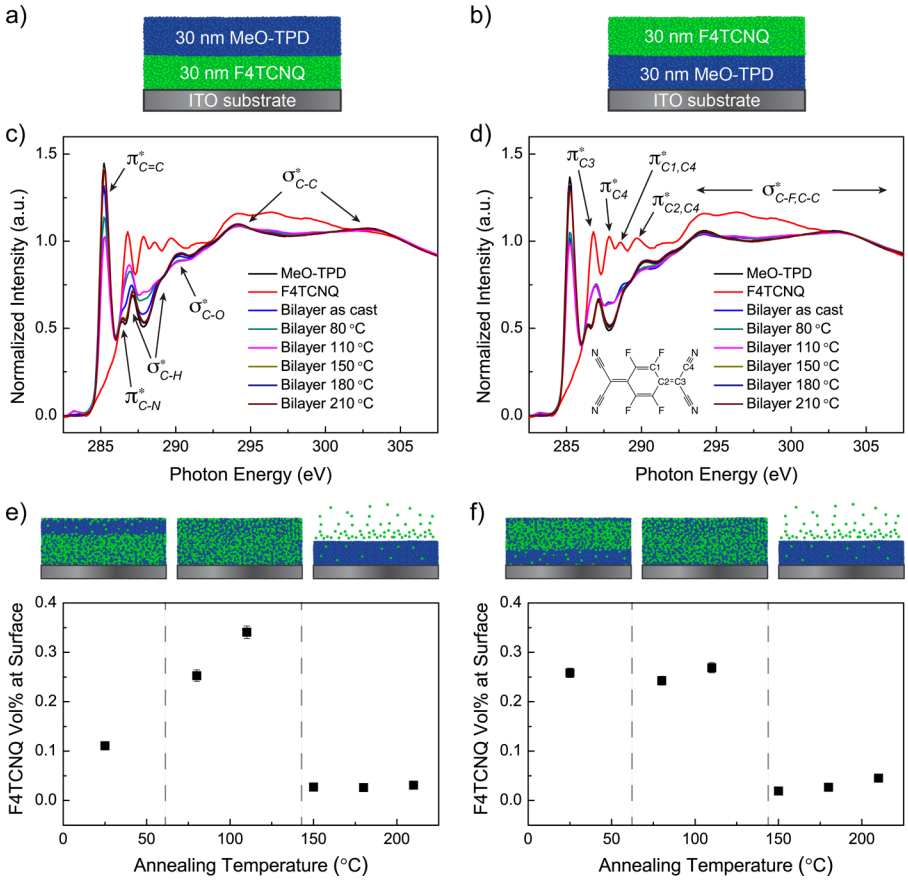

Figure 7. Carbon K-edge NEXAFS spectra of bilayers of 30 nm MeO-TPD (blue) evaporated onto 30 nm F4TCNQ (green) (a, c) and F4TCNQ evaporated onto MeO-TPD (b, d). The bilayers were measured as deposited (blue) and thermally annealed at 80 °C (cyan), 110 °C (magenta), 150 °C (dark yellow), 180 °C (navy), and 210 °C (wine). The peak assignments of MeO-TPD and F4TCNQ are shown in panels c and d, respectively. The NEXAFS spectra of bilayers were fit using the neat MeO-TPD and dopant spectra. This fit represents a fitting of the volume fraction of dopant material within the escape depth of the backscattered electron (~4 nm) and is plotted in panel e for MeO-TPD/F4TCNQ and in panel f for F4TCNQ/MeO-TPD.

sharp interface between the two materials implies that MeO-TPD used with $C_{60}F_{36}$ has a more stable morphology than with F4TCNQ, which is consistent with the spectroscopy results. The high SLD at the substrate interface is likely due to the presence of a high density $C_{60}F_{36}$ interlayer. After heating the sample at 110 °C for 5 min, two distinct layers remain intact and only some slight interfacial mixing is observed. Similar results were also reported for TIPS-DBC/C_{60} bilayer using X-ray reflectometry (XRR).[48] The high SLD of the sample surface is also attributed to the low surface energy of dopant and thermal oxidation. To demonstrate the diffusion of dopants in general, we also performed XRR experiments on HTL/dopant/HTL trilayer samples, the details of which are provided in the Supporting Information (Figure S3).

Near-Edge X-ray Absorption Fine Structure. NEXAFS spectroscopy is another technique that we used to observe the diffusion of the dopants. Electron yield NEXAFS is a surface specific measurement that characterizes the top ~4 nm of the film due to the limited escape depth of the electrons. By carefully investigating the dopants/HTL bilayer samples and their inverse structures, we are able to provide a comprehensive picture on the diffusion of both materials.

In this section, the diffusion of F4TCNQ molecules in MeO-TPD will first be investigated: a bilayer of a 30 nm MeO-TPD layer on top of 30 nm of F4TCNQ (MeO-TPD/F4TCNQ) and its inverse structure (F4TCNQ/MeO-TPD) were fabricated, as shown in Figure 7a,b, respectively. The normalized carbon K-edge TEY spectra of both structures before and after annealing are shown in Figure 7c,d. The spectra of neat MeO-TPD and F4TCNQ are also plotted for reference. The characteristic peaks of MeO-TPD can be assigned based on the work of Watts et al.[33] The first peak at 285.2 eV corresponds to the C 1s (C═C) → $\pi^*_{C=C}$ resonance associated with aromatic carbons in the benzenoid rings. The small shoulder around 286.4 eV is assigned as a C 1s (C−N) → π^*_{C-N} transition. The peak at 287.1 eV and the shoulder at 288.8 eV are due to a C 1s (C−H) → σ^*_{C-H} transition. The noticeable shoulder around 290.1 eV is from C 1s (C−O) → σ^*_{C-H}. The C 1s (C−C) → σ^*_{C-C} features are shown above 293 eV. For F4TCNQ, studies have already shown that multiple peaks below 293 eV are due to C 1s → π^* transitions while the broad features above 293 eV are attributed to σ^*_{C-C} and σ^*_{C-F} excitations.[49] The specific peak assignments of MeO-TPD and F4TCNQ are shown in Figure 7c,d, respectively.

To determine the volume percent change of each component at the surface as a function of annealing temperature, the NEXAFS spectra of the bilayers were fit using the linear combination method. Two fits, one with forcing weights to sum to 1 and one without, were performed, and the corresponding results are provided in the Supporting Information (Figures S4−S7 and Tables S1−S4). Given the decent two-component

DOI: 10.1021/acsami.5b09216
ACS Appl. Mater. Interfaces 2015, 7, 28420−28428

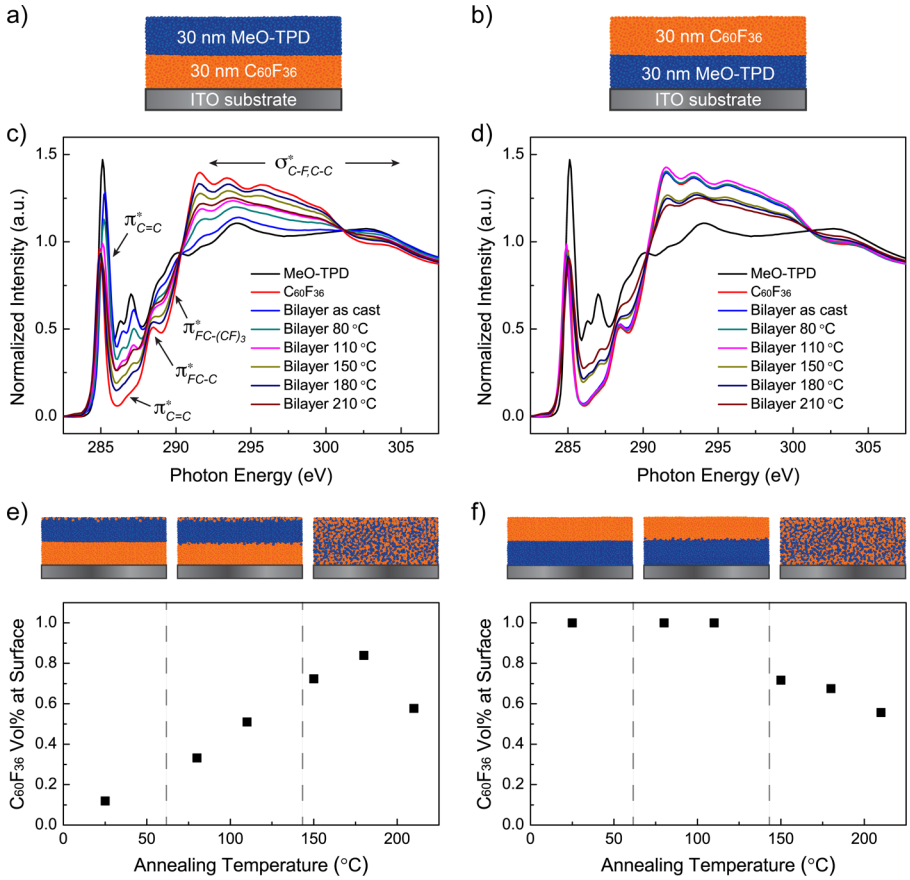

Figure 8. Carbon K-edge NEXAFS spectra of bilayers of 30 nm MeO-TPD (blue) evaporated onto 30 nm $C_{60}F_{36}$ (green) (a, c) and $C_{60}F_{36}$ evaporated onto MeO-TPD (b, d). The bilayers were measured as deposited (blue) and thermally annealed at 80 °C (cyan), 110 °C (magenta), 150 °C (dark Yellow), 180 °C (navy), and 210 °C (wine). The peak assignments of $C_{60}F_{36}$ is shown in panel c. The NEXAFS spectra of bilayers were fit using the neat MeO-TPD and dopant spectra. This fit represents a fitting of the volume fraction of dopant material within the escape depth of the backscattered electron (~4 nm) and is plotted in panel e for MeO-TPD/$C_{60}F_{36}$ and in panel f for $C_{60}F_{36}$/MeO-TPD.

fits (small χ^2 values) and only subtle differences between these two fit results, we can assume that doping only has a small contribution to the total NEXAFS spectrum (<3%). The fitted volume fraction of dopant material at the surface is plotted in Figure 7e,f. This surface compositional information combined with optical spectroscopy and NR results mentioned earlier provide a comprehensive picture on the F4TCNQ diffusion in MeO-TPD upon thermal annealing (see the cartoons in Figure 7e,f). Three distinct temperature regimes are established. Before thermal annealing, diffusion of F4TCNQ has taken place spontaneously, mixing and doping with MeO-TPD. A small portion of F4TCNQ accumulates at the surface due to its low surface energy. Upon thermal annealing up to 110 °C, F4TCNQ is able to diffuse all the way through the MeO-TPD layer, and a highly doped homogeneous layer is formed. Above 150 °C, F4TCNQ starts to sublimate and only a trace of F4TCNQ can be detected in the film after heating to 180 °C.

Following the same procedure, the diffusion of $C_{60}F_{36}$ molecules in MeO-TPD can also be investigated. The bilayer structures of MeO-TPD/$C_{60}F_{36}$ and $C_{60}F_{36}$/MeO-TPD are shown in Figure 8a,b, respectively. The carbon K-edge NEXAFS spectra and their corresponding fit results are presented in Figure 8c–f. The characteristic peaks of $C_{60}F_{36}$ can be assigned based on the work of Bulusheva et al.[50] The high intensity peak at 284.9 eV and the small peak at 286.8 eV are assigned as C 1s → $\pi^*_{C=C}$ transitions associated with carbon–carbon bonds in the benzenoid rings and double carbon bonds. The peak at 288.5 eV is due to C 1s → π^*_{FC-C} transition which corresponds to the bonding of the fluorinated carbon atom with bare carbons. The shoulder around 289.6 eV is due to C 1s → $\pi^*_{FC-(CF)\,3}$ resonance corresponding to the bonding of the fluorinated carbon atom with three CF groups. The features above 291 eV are due to C 1s → σ^* transitions. Similarly, a comprehensive scheme on the diffusion of $C_{60}F_{36}$ in MeO-TPD upon thermal annealing is provided (see the cartoons in Figure 8e,f). Unlike F4TCNQ, two distinct layers of $C_{60}F_{36}$ and MeO-TPD remain intact up to 110 °C. Interestingly, even for the room temperature $C_{60}F_{36}$/MeO-TPD sample some $C_{60}F_{36}$ is detected at the surface. This means that instead of covering the $C_{60}F_{36}$ layer, the MeO-TPD got under a monolayer of $C_{60}F_{36}$ and formed under the monolayer. Even after 30 nm of MeO-TPD evaporation, there is still $C_{60}F_{36}$ at the surface. This clearly shows that even for dopants that are thermally stable, the initially deposited sample has a significantly different interface concentration than expected. Increasing the annealing temperature to 110 °C results in slightly increased $C_{60}F_{36}$ content at the surface, which indicates that the dopant diffused through the MeO-TPD layer but was trapped at the surface. The accumulation of $C_{60}F_{36}$ at the surface of MeO-TPD/$C_{60}F_{36}$ is also due to the low surface energy of dopant molecules. Starting at 150 °C, a threshold temperature is reached at which the materials mix completely.

The differences in the diffusion rates of F4TCNQ and $C_{60}F_{36}$ through MeO-TPD are likely due to both the differences in

DOI: 10.1021/acsami.5b09216
ACS Appl. Mater. Interfaces 2015, 7, 28420−28428

molecular size/geometry and thermal properties of the two dopant molecules. Given the smaller size ($V_{m\,F4TCNQ}$ = 172.6 cm^3/mol vs $V_{m\,C_{60}F_{36}}$ = 739.3 cm^3/mol) and the more planar structure of the F4TCNQ, it can more easily move through the void space and interstitial sites within the MeO-TPD material. The diffusion of F4TCNQ was shown to occur at ambient temperatures. For mild temperatures, the diffusion rate of the F4TCNQ increased substantially, while the diffusion of the $C_{60}F_{36}$ remained low. This undesired diffusion of dopants in hole transport layers has been known to be a contributing cause of an increase in recombination centers that degrade device performance.[36,51−53]

CONCLUSION

The thermal stability of bilayers of MeO-TPD and molecular dopants, F4TCNQ and $C_{60}F_{36}$, was investigated because it has been observed that molecular dopants can diffuse within organic electronic devices, to the detriment of the device. Here UV−vis−near-IR spectroscopy, photoluminescence spectroscopy, neutron reflectometry, and near-edge X-ray absorption fine structure spectroscopy were used to determine the movement of dopants through the layer stack. There was a substantial amount of mixing between the MeO-TPD and F4TCNQ even at room temperature. While the bilayer appears to have little initial mixing, we were able to detect the movement of the dopant into the MeO-TPD over a period of days. The sample was completely mixed with annealing to 110 °C. The MeO-TPD and $C_{60}F_{36}$ bilayer has higher thermal stability with moderate heating. At 150 °C the sample becomes completely mixed. This result validates the use of $C_{60}F_{36}$ as a desirable alternative to the less thermally stable F4TCNQ. Studies of degradation processes, such as molecular diffusion, are important for understanding organic device longevity and the associated breakdown mechanisms.

ASSOCIATED CONTENT

Supporting Information

The Supporting Information is available free of charge on the ACS Publications website at DOI: 10.1021/acsami.5b09216.

UV−vis−near-IR and photoluminescence spectra, XRR, and carbon K-edge NEXAFS. (PDF)

AUTHOR INFORMATION

Corresponding Author

*E-mail: amoule@ucdavis.edu.

Notes

The authors declare no competing financial interest.

ACKNOWLEDGMENTS

This project was carried out with funding from the U.S. Department of Energy (DOE), Office of Basic Energy Sciences, Division of Materials Sciences and Engineering, under Award No. DE-SC0010419. M. Riede was supported from BMBF, Innoprofile 03IP602 Programme. This work benefited from the use of the Lujan Neutron Scattering Center at LANSCE funded by the DOE Office of Basic Energy Sciences and Los Alamos National Laboratory (LANL) under DOE Contract DE-AC52-06NA25396. We thank Jaroslaw Majewski from the LANL for user support and training. Part of this work was performed under the auspices of the U.S. Department of Energy by Lawrence Livermore National Laboratory (LLNL) under Contract DE-AC52-07NA27344. We also would like to thank Michael Toney from Stanford Synchrotron Radiation Lightsource (SSRL) for user support and XRR training.

REFERENCES

(1) Braga, D.; Horowitz, G. High-Performance Organic Field-Effect Transistors. *Adv. Mater.* **2009**, *21*, 1473−1486.

(2) Hains, A. W.; Liang, Z.; Woodhouse, M. A.; Gregg, B. A. Molecular Semiconductors in Organic Photovoltaic Cells. *Chem. Rev.* **2010**, *110*, 6689−6735.

(3) Xu, M. F.; Shi, X. B.; Jin, Z. M.; Zu, F. S.; Liu, Y.; Zhang, L.; Wang, Z. K.; Liao, L. S. Aqueous Solution-Processed GeO2: An Anode Interfacial Layer for High Performance and Air-Stable Organic Solar Cells. *ACS Appl. Mater. Interfaces* **2013**, *5*, 10866−10873.

(4) Aziz, H.; Popovic, Z. D.; Hu, N.-X.; Hor, A-M.; Xu, G. Degradation Mechanism of Small Molecule-Based Organic Light-Emitting Devices. *Science* **1999**, *283*, 1900−1902.

(5) Hu, T.; Li, F.; Yuan, K.; Chen, Y. Efficiency and Air-Stability Improvement of Flexible Inverted Polymer Solar Cells Using ZnO/Poly(ethylene glycol) Hybrids as Cathode Buffer Layers. *ACS Appl. Mater. Interfaces* **2013**, *5*, 5763−5770.

(6) Jørgensen, M.; Norrman, K.; Gevorgyan, S. A.; Tromholt, T.; Andreasen, B.; Krebs, F. C. Stability of Polymer Solar Cells. *Adv. Mater.* **2012**, *24*, 580−612.

(7) Lee, J. U.; Jung, J. W.; Jo, J. W.; Jo, W. H. Degradation and Stability of Polymer-Based Solar Cells. *J. Mater. Chem.* **2012**, *22*, 24265−24283.

(8) Zhao, X.; Zhan, X. Electron Transporting Semiconducting Polymers in Organic Electronics. *Chem. Soc. Rev.* **2011**, *40*, 3728−3743.

(9) Hains, A. W.; Marks, T. J. High-Efficiency Hole Extraction/Electron-Blocking Layer to Replace Poly(3,4-ethylenedioxythiophene):Poly(styrene sulfonate) in Bulk-Heterojunction Polymer Solar Cells. *Appl. Phys. Lett.* **2008**, *92*, 023504.

(10) Huang, J.; Pfeiffer, M.; Werner, A.; Blochwitz, J.; Leo, K.; Liu, S. Low-Voltage Organic Electroluminescent Devices Using *pin* Structures. *Appl. Phys. Lett.* **2002**, *80*, 139−141.

(11) Lüssem, B.; Riede, M.; Leo, K. Doping of Organic Semiconductors. *Phys. Status Solidi A* **2013**, *210*, 9−43.

(12) Tietze, M. L.; Burtone, L.; Riede, M.; Lussem, B.; Leo, K. Fermi Level Shift and Doping Efficiency in *p*-Doped Small Molecule Organic Semiconductors: A Photoelectron Spectroscopy and Theoretical Study. *Phys. Rev. B: Condens. Matter Mater. Phys.* **2012**, *86*, 035320.

(13) Zhou, X.; Blochwitz, J.; Pfeiffer, M.; Nollau, A.; Fritz, T.; Leo, K. Enhanced Hole Injection into Amorphous Hole-Transport Layers of Organic Light-Emitting Diodes Using Controlled p-Type Doping. *Adv. Funct. Mater.* **2001**, *11*, 310−314.

(14) Guo, S.; Kim, S. B.; Mohapatra, S. K.; Qi, Y. B.; Sajoto, T.; Kahn, A.; Marder, S. R.; Barlow, S. N-Doping of Organic Electronic Materials Using Air-Stable Organometallics. *Adv. Mater.* **2012**, *24*, 699−703.

(15) Meerheim, R.; Walzer, K.; Pfeiffer, M.; Leo, K. Ultrastable and Efficient Red Organic Light Emitting Diodes with Doped Transport Layers. *Appl. Phys. Lett.* **2006**, *89*, 061111.

(16) Yu, Y. J.; Solomeshch, O.; Chechik, H.; Goryunkov, A. A.; Tuktarov, R. F.; Choi, D. H.; Jin, J. I.; Eichen, Y.; Tessler, N. P-Type Doping in Organic Light Emitting Diodes Based on Fluorinated C60. *J. Appl. Phys.* **2008**, *104*, 124505.

(17) Naab, B. D.; Guo, S.; Olthof, S.; Evans, E. G. B.; Wei, P.; Millhauser, G. L.; Kahn, A.; Barlow, S.; Marder, S. R.; Bao, Z. Mechanistic Study on the Solution-Phase N-Doping of 1,3-Dimethyl-2-aryl-2,3-dihydro-1H-benzoimidazole Derivatives. *J. Am. Chem. Soc.* **2013**, *135*, 15018−15025.

(18) Bruder, I.; Watanabe, S.; Qu, J. Q.; Muller, I. B.; Kopecek, R.; Hwang, J.; Weis, J.; Langer, N. A Novel P-Dopant with Low Diffusion Tendency and Its Application to Organic Light-Emitting Diodes. *Org. Electron.* **2010**, *11*, 589−593.

(19) Arkhipov, V. I.; Emelianova, E. V.; Bassler, H. Quenching of Excitons in Doped Disordered Organic Semiconductors. *Phys. Rev. B: Condens. Matter Mater. Phys.* **2004**, *70*, 205205.
(20) Brédas, J.; Wudl, F.; Heeger, A. Polarons and Bipolarons in Doped Polythiophene: A Theoretical Investigation. *Solid State Commun.* **1987**, *63*, 577−580.
(21) Colaneri, N.; Nowak, M.; Spiegel, D.; Hotta, S.; Heeger, A. J. Bipolarons in Poly(3-methylthiophene): Spectroscopic, Magnetic, and Electrochemical Measurements. *Phys. Rev. B: Condens. Matter Mater. Phys.* **1987**, *36*, 7964−7968.
(22) Parthasarathy, G.; Shen, C.; Kahn, A.; Forrest, S. R. Lithium Doping of Semiconducting Organic Charge Transport Materials. *J. Appl. Phys.* **2001**, *89*, 4986−4992.
(23) Kido, J.; Matsumoto, T. Bright Organic Electroluminescent Devices Having A Metal-Doped Electron-Injecting Layer. *Appl. Phys. Lett.* **1998**, *73*, 2866−2868.
(24) Zhang, Y.; de Boer, B.; Blom, P. W. M. Controllable Molecular Doping and Charge Transport in Solution-Processed Polymer Semiconducting Layers. *Adv. Funct. Mater.* **2009**, *19*, 1901−1905.
(25) Duong, D. T.; Wang, C.; Antono, E.; Toney, M. F.; Salleo, A. The Chemical and Structural Origin of Efficient P-Type Doping in P3HT. *Org. Electron.* **2013**, *14*, 1330−1336.
(26) Li, J.; Zhang, G.; Holm, D. M.; Jacobs, I. E.; Yin, B.; Stroeve, P.; Mascal, M.; Moulé, A. J. Introducing Solubility Control for Improved Organic P-Type Dopants. *Chem. Mater.* **2015**, *27*, 5765−5774.
(27) Mi, B. X.; Gao, Z. Q.; Cheah, K. W.; Chen, C. H. Organic Light-Emitting Diodes Using 3,6-Difluoro-2,5,7,7,8,8-hexacyanoquinodimethane As P-Type Dopant. *Appl. Phys. Lett.* **2009**, *94*, 073507.
(28) Meerheim, R.; Olthof, S.; Hermenau, M.; Scholz, S.; Petrich, A.; Tessler, N.; Solomeshch, O.; Lüssem, B.; Riede, M.; Leo, K. Investigation of C60F36 as Low-Volatility P-Dopant in Organic Optoelectronic Devices. *J. Appl. Phys.* **2011**, *109*, 103102.
(29) Solomeshch, O.; Yu, Y. J.; Goryunkov, A. A.; Sidorov, L. N.; Tuktarov, R. F.; Choi, D. H.; Jin, J. I.; Tessler, N. Ground State Interaction and Electrical Doping of Fluorinated C60 in Conjugated Polymers. *Adv. Mater.* **2009**, *21*, 4456−4460.
(30) Dubey, M.; Jablin, M. S.; Wang, P.; Mocko, M.; Majewski, J. SPEAR-ToF Neutron Reflectometer at the Los Alamos Neutron Science Center. *Eur. Phys. J. Plus* **2011**, *126*, 110.
(31) Nelson, A. Co-Refinement of Multiple-Contrast Neutron/X-ray Reflectivity Data Using MOTOFIT. *J. Appl. Crystallogr.* **2006**, *39*, 273−276.
(32) *Scattering Length Density Calculator*, National Institute of Standards and Technology (NIST) Center for Neutron Research, http://www.ncnr.nist.gov/resources/sldcalc.html (accessed Sep. 12, 2015).
(33) Watts, B.; Swaraj, S.; Nordlund, D.; Lüning, J.; Ade, H. Calibrated NEXAFS Spectra of Common Conjugated Polymers. *J. Chem. Phys.* **2011**, *134*, 024702.
(34) Gao, J.; Roehling, J. D.; Li, Y.; Guo, H.; Moule, A. J.; Grey, J. K. The Effect of 2,3,5,6-Tetrafluoro-7,7,8,8-tetracyanoquinodimethane Charge Transfer Dopants on the Conformation and Aggregation of Poly(3-hexylthiophene). *J. Mater. Chem. C* **2013**, *1*, 5638−5646.
(35) Mendez, H.; Heimel, G.; Opitz, A.; Sauer, K.; Barkowski, P.; Oehzelt, M.; Soeda, J.; Okamoto, T.; Takeya, J.; Arlin, J. B.; Balandier, J. Y.; Geerts, Y.; Koch, N.; Salzmann, I. Doping of Organic Semiconductors: Impact of Dopant Strength and Electronic Coupling. *Angew. Chem., Int. Ed.* **2013**, *52*, 7751−7755.
(36) Lee, J. H.; Lee, J.; Kim, Y. H.; Yun, C.; Lüssem, B.; Leo, K. Effect of Trap States on the Electrical Doping of Organic Semiconductors. *Org. Electron.* **2014**, *15*, 16−21.
(37) Melby, L. R.; Harder, R. J.; Hertler, W. R.; Mahler, W.; Benson, R. E.; Mochel, W. E. Substituted Quinodimethans. II. Anion-radical Derivatives and Complexes of 7,7,8,8-Tetracyanoquinodimethan. *J. Am. Chem. Soc.* **1962**, *84*, 3374−3387.
(38) Li, F.; Werner, A.; Pfeiffer, M.; Leo, K.; Liu, X. Leuco Crystal Violet as a Dopant for N-Doping of Organic Thin Films of Fullerene C60. *J. Phys. Chem. B* **2004**, *108*, 17076−17082.
(39) Gao, Z. Q.; Xia, P. F.; Lo, P. K.; Mi, B. X.; Tam, H. L.; Wong, M. S.; Cheah, K. W.; Chen, C. H. P-Doped P-Phenylenediamine-Substituted Fluorenes for Organic Electroluminescent Devices. *Org. Electron.* **2009**, *10*, 666−673.
(40) Wei, P.; Menke, T.; Naab, B. D.; Leo, K.; Riede, M.; Bao, Z. 2-(2-Methoxyphenyl)-1,3-dimethyl-1H-benzoimidazol-3-ium Iodide as A New Air-Stable N-Type Dopant for Vacuum-Processed Organic Semiconductor Thin Films. *J. Am. Chem. Soc.* **2012**, *134*, 3999−4002.
(41) Gao, Z. Q.; Mi, B. X.; Xu, G. Z.; Wan, Y. Q.; Gong, M. L.; Cheah, K. W.; Chen, C. H. An Organic P-Type Dopant with High Thermal Stability for An Organic Semiconductor. *Chem. Commun.* **2008**, *1*, 117−119.
(42) Pfeiffer, M.; Leo, K.; Zhou, X.; Huang, J.; Hofmann, M.; Werner, A.; Blochwitz-Nimoth, J. Doped Organic Semiconductors: Physics and Application in Light Emitting Diodes. *Org. Electron.* **2003**, *4*, 89−103.
(43) Wellmann, P.; Hofmann, M.; Zeika, O.; Werner, A.; Birnstock, J.; Meerheim, R.; He, G.; Walzer, K.; Pfeiffer, M.; Leo, K. High-Efficiency p-i-n Organic Light-Emitting Diodes with Long Lifetime. *J. Soc. Inf. Disp.* **2005**, *13*, 393−397.
(44) Yim, K. H.; Whiting, G. L.; Murphy, C. E.; Halls, J. J. M.; Burroughes, J. H.; Friend, R. H.; Kim, J.-S. Controlling Electrical Properties of Conjugated Polymers via A Solution-Based P-Type Doping. *Adv. Mater.* **2008**, *20*, 3319−3324.
(45) Tsoi, W. C.; Spencer, S. J.; Yang, L.; Ballantyne, A. M.; Nicholson, P. G.; Turnbull, A.; Shard, A. G.; Murphy, C. E.; Bradley, D. D. C.; Nelson, J.; Kim, J.-S. Effect of Crystallization on the Electronic Energy Levels and Thin Film Morphology of P3HT:PCBM Blends. *Macromolecules* **2011**, *44*, 2944−2952.
(46) Huang, D. M.; Mauger, S. A.; Friedrich, S.; George, S. J.; Dumitriu-LaGrange, D.; Yoon, S.; Moulé, A. J. The Consequences of Interface Mixing on Organic Photovoltaic Device Characteristics. *Adv. Funct. Mater.* **2011**, *21*, 1657−1665.
(47) Mauger, S. A.; Li, J.; Ozmen, O. T.; Yang, A. Y.; Friedrich, S.; Rail, M. D.; Berben, L. A.; Moule, A. J. High Work-Function Hole Transport Layers by Self-Assembly Using a Fluorinated Additive. *J. Mater. Chem. C* **2014**, *2*, 115−123.
(48) Scholes, F. H.; Ehlig, T.; James, M.; Lee, K. H.; Duffy, N.; Scully, A. D.; Singh, T. B.; Winzenberg, K. N.; Kemppinen, P.; Watkins, S. E. Intraphase Microstructure-Understanding the Impact on Organic Solar Cell Performance. *Adv. Funct. Mater.* **2013**, *23*, 5655−5662.
(49) Koshino, M.; Kurata, H.; Isoda, S. DV-Xα Calculation of Electron Energy-Loss Near Edge-Structures of 2,3,5,6-Tetrafluoro-7,7,8,8-tetracyanoquinodimethane (F4TCNQ). *J. Electron Spectrosc. Relat. Phenom.* **2004**, *135*, 191−200.
(50) Bulusheva, L. G.; Okotrub, A. V.; Shnitov, V. V.; Bryzgalov, V. V.; Boltalina, O. V.; Gol'dt, I. V.; Vyalikh, D. V. Electronic Structure of C60F36 Studied by Quantum-Chemical Modeling of Experimental Photoemission and X-Ray Absorption Spectra. *J. Chem. Phys.* **2009**, *130*, 014704.
(51) Gao, W.; Kahn, A. Controlled *p* Doping of the Hole-Transport Molecular Material N,N′-Diphenyl-N,N′-bis(1-naphthyl)-1,1′-biphenyl-4,4′-diamine with Tetrafluorotetracyanoquinodimethane. *J. Appl. Phys.* **2003**, *94*, 359−366.
(52) Walzer, K.; Maennig, B.; Pfeiffer, M.; Leo, K. Highly Efficient Organic Devices Based on Electrically Doped Transport Layers. *Chem. Rev.* **2007**, *107*, 1233−1271.
(53) Olthof, S.; Tress, W.; Meerheim, R.; Lüssem, B.; Leo, K. Photoelectron Spectroscopy Study of Systematically Varied Doping Concentrations in An Organic Semiconductor Layer Using A Molecular P-Dopant. *J. Appl. Phys.* **2009**, *106*, 103711.

DOI: 10.1021/acsami.5b09216
ACS Appl. Mater. Interfaces 2015, 7, 28420−28428